3D Millimeter-Wave Peer-to-Peer Networks With Boundary Located Destination

Massimiliano Comisso, Francesca Vatta, Giulia Buttazzoni, and Fulvio Babich

***Abstract*— This letter presents a theoretical analysis for estimating the coverage probability and the average link capacity of an interfered peer-to-peer millimeter-wave communication when the destination lies at the boundary of a three-dimensional cell. The proposed model provides closed-form expressions for the statistics of the desired and undesired signal powers, by accounting for the impact of directional antenna gains, path-loss attenuation, mid-scale fading, interference, and noise.**

***Index Terms*— Millimeter-wave, peer-to-peer, link capacity, cell boundary, 3D analysis.**

I. Introduction

FIFTH-GENERATION (5G) cellular networks are expected to represent a cornerstone for the evolution of radiomobile networks, not only in terms of system capacity, through the exploitation of the millimeter-wave (mmWave) bands, but also in terms of available functionalities, through the introduction of device-to-device communications [1]. This novel functionality, combined with the ultra-densification strategy adopted for the 5G base stations, depicts a challenging context characterized by the coexistence, within a unique cell, of many concurrent, and hence reciprocally interfering, peer-to-peer (P2P) links. In this situation, the usual uplink model, in which the destination lies at the center of a cell, is no more sufficient to exhaustively characterize the result of a P2P communication, since the destination may also lie at the boundary of the cell. This asymmetric scenario has been previously analyzed by modeling the cell as a two-dimensional disk, in order to evaluate the statistic of the interference power [2], and the coverage probability [3]. However, in the specific 5G case, the involved nodes might also lie overground or underground relative to one another, as a consequence of the short communication distances. Besides, from a massive multiple input multiple output (MIMO) perspective, the availability of antenna systems with azimuth and zenith beam steering capabilities allows the exploitation of the entire three-dimensional (3D) domain, and, in turn, the increase of the link capacity. This makes desirable the development of 3D mmWave network models [4], [5], within which the possible boundary location of the destination has not been even considered.

Manuscript received February 26, 2019; revised April 4, 2019; accepted April 30, 2019. Date of publication May 7, 2019; date of current version July 10, 2019. This work is partly supported by the Italian Ministry of University and Research (MIUR), project FRA 2018 (Univ. of Trieste): "UBER-5G: Cubesat 5G networks—Access layer analysis and antenna system development." The associate editor coordinating the review of this letter and approving it for publication was R. He. *(Corresponding author: Massimiliano Comisso.)*

The authors are with the Department of Engineering and Architecture, University of Trieste, 34127 Trieste, Italy (e-mail: mcomisso@units.it).

To deal with this issue, this letter analyzes an interfered P2P mmWave communication by comparing the cases of centered and boundary located destination. The analysis, which is validated by numerical simulations, adopts an experimentally assessed 3D mmWave channel model including path-loss attenuation and shadowing. Closed-form expressions for the statistics of the desired and undesired signal powers are derived, with the final aim of identifying the link capacity variation introduced by the asymmetric position of the destination.

The letter is organized as follows. Section II introduces the scenario. Section III presents the analysis. Section IV discusses the results. Section V summarizes the conclusions.

Notation. Throughout the letter the following notation is used: $\mathbb{R}_{>0}$ denotes the set of positive reals, δ_{ij} denotes the Kronecker delta ($\delta_{ij}=1$ if $i=j$, $\delta_{ij}=0$ otherwise), $\mathbb{1}_{\mathbf{X}}(\mathbf{x})$ denotes the indicator function ($\mathbb{1}_{\mathbf{X}}(\mathbf{x})=1$ if $\mathbf{x}\in\mathbf{X}$, $\mathbb{1}_{\mathbf{X}}(\mathbf{x})=0$ otherwise), $(\cdot)^+$ denotes the positive part, $\delta(\cdot)$ denotes the Dirac delta function, $\mathrm{erf}(\cdot)$ denotes the error function, $\mathbb{E}_X[\cdot]$ denotes the expectation over a random variable (rv) X.

II. System Model

Consider a 3D ball $\mathbf{B}(O,\rho)$ of center O and radius ρ, in which L P2P communications, that is, L sources S_l ($l=1,\ldots,L$) and their destinations, are simultaneously active. The L value is the realization of a Poisson-distributed rv $\mathcal{L}$ having probability density function (pdf) [6]:

$$f_{\mathcal{L}}(L)=\frac{\lambda^L}{L!}\exp(-\lambda),\quad L=0,1,\ldots \tag{1}$$

where λ is the average number of active sources. Denote by S_1 a target source, by D its destination, and by $\mathrm{S}_{l\neq 1}$ one of the other sources, perceived by D as interferers. The position of S_l with respect to D is described by the random vector $\mathbf{R}_l=(R_l,\Theta_l,\Phi_l)$, where the rvs R_l, Θ_l, and Φ_l represent the distance and the zenith/azimuth angles, respectively. The L sources are uniformly distributed inside $\mathbf{B}(O,\rho)$, and a parameter s is used to identify two positions for D: the center O (case $s=1$, Fig. 1(a)), and the boundary of $\mathbf{B}(O,\rho)$ (case $s=2$, Fig. 1(b)). For these positions, the pdf of $\mathbf{R}_l$ with respect to D can be written in spherical coordinates as [6]:

$$f_{\mathbf{R}_l}(\mathbf{r}_l;s)=\frac{3r_l^2\sin\theta_l}{4\pi\rho^3}\,\mathbb{1}_{\mathbf{Z}_s}(\mathbf{r}_l),\quad s=1,2;\ l=1,\ldots,L \tag{2}$$

where the point of observation identifies the domain:

$$\mathbf{Z}_s=\begin{cases}[0,\rho]\times[0,\pi]\times[0,2\pi) & s=1\\ [0,-2\rho\sin\theta_l\cos\phi_l]\times[0,\pi]\times[\pi/2,3\pi/2] & s=2\end{cases} \tag{3}$$

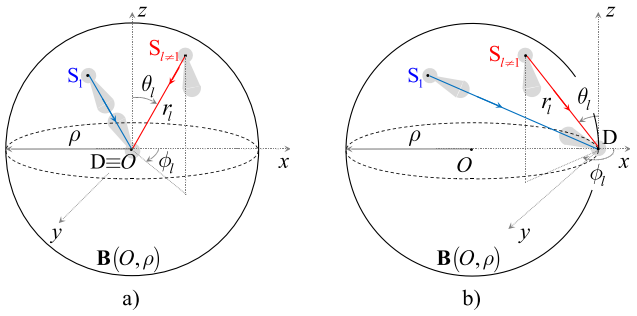

Fig. 1. Target destination D located at (a) the center and (b) the boundary of a 3D ball (S_1: target source, $S_{l\neq 1}$: generic interfering source).

This spatial statistic is combined with the mmWave channel model experimentally assessed in [4], which includes shadowing and relies on the floating-intercept path-loss model. Small-scale fading is neglected for its lower significance in mmWave communications [7]. Accordingly, the rv describing the power received by D from S_l is expressed as [4]:

$$P_l = \frac{P_T G_{T_l} G_{R_l}}{\alpha R_l^{\beta}} \Psi_l, \quad l=1,\dots,L \tag{4}$$

where P_T is the transmission power, G_{T_l} is the transmitting antenna gain of S_l towards D, G_{R_l} is the receiving antenna gain of D towards S_l, α is the floating intercept, β is the path-loss exponent, and Ψ_l is a log-normal rv with pdf [7]:

$$f_{\Psi_l}(\psi_l) = \frac{1}{\sqrt{2\pi}\tilde{\sigma}\psi_l} \exp\left(-\frac{\log^2 \psi_l}{2\tilde{\sigma}^2}\right) \mathbb{1}_{\mathbb{R}_{>0}}(\psi_l), \tag{5}$$

in which $\tilde{\sigma}$ is the shadowing standard deviation.

In a P2P scenario, all nodes reasonably employ the same directional antenna pattern, which, adopting the flat-top model, can be described by its main lobe beamwidth Ω, its maximum gain $\mathfrak{G}$, and its backlobe gain $\mathfrak{g}$. To support the target link, S_1 and D steer towards each other their main beams, but in the presence of a zero-mean $\hat{\sigma}^2$-variance Gaussian beamsteering error [7]. The direction of an interferer $S_{l\neq 1}$ and the direction from which this interferer is received by D are instead both random. Thus, for $N \in \{T, R\}$, G_{N_l} in (4) is a rv with pdf [7]:

$$f_{G_{N_l}}(g_{N_l}) = K_l(\Omega)\delta(g_{N_l} - \mathfrak{G}) + [1 - K_l(\Omega)]\delta(g_{N_l} - \mathfrak{g}), \tag{6}$$

where:

$$K_l(\Omega) = \begin{cases} \operatorname{erf}\left[\Omega/(2\sqrt{2}\hat{\sigma})\right] & l = 1 \\ \Omega/(4\pi) & l \neq 1 \end{cases} \tag{7}$$

Beside the interference incoming from $S_2,\dots,S_L$, the target link is subject to a noise power $\mathcal{N}$. Its performance is estimated considering an adaptive system modeled through the Shannon bound, and, alternatively, a practical one using a fixed quadrature phase-shift keying (QPSK) modulation. For these systems, the capacity as a function of the signal to interference plus noise ratio (SINR) ξ may be expressed as [8]:

$$\mathcal{M}_m(\xi) = \begin{cases} \log_2(1+\xi) & m=1 \text{ (Shannon)} \\ 2\left[1-\exp(\varsigma_1 - \varsigma_2 \xi^{\varsigma_3})\right]^+ & m=2 \text{ (QPSK)} \end{cases} \tag{8}$$

where $\varsigma_1 \cong 0.0102$, $\varsigma_2 \cong 0.6746$, $\varsigma_3 \cong 0.9308$.

The above introduced scenario is analyzed in the next section to identify the impact of the destination's location on the average capacity of the $S_1 - D$ P2P link.

III. Analysis

The analysis is carried out in three steps. The first step aims to derive the distance distribution for the two positions of D. This task is accomplished through the following lemma.

Lemma 1 (Distance distribution): Let $\mathbf{R}_l$ be distributed according to (2)-(3). Then, for $s = 1, 2$ and $l = 1,\dots,L$, the cumulative distribution function (cdf) of R_l is given by:

$$F_{R_l}(r_l; s) = \left(\sum_{n=1}^{2} a_n^s r_l^{n+2}\right) \mathbb{1}_{(0,s\rho]}(r_l) + \mathbb{1}_{(s\rho,+\infty)}(r_l), \tag{9}$$

where:

$$a_n^s = \frac{1-(n-1)s}{s\rho^3}\left(\frac{3}{8\rho}\right)^{n-1}, \quad n = 1, 2. \tag{10}$$

Proof: For $s = 1$, the pdf of R_l can be directly evaluated considering $\mathbf{Z}_1$ in (3), thus obtaining:

$$f_{R_l}(r_l; 1) = \frac{3r_l^2}{4\pi\rho^3} \int_0^{\pi} \sin\theta_l \mathrm{d}\theta_l \int_0^{2\pi} \mathrm{d}\phi_l = 3a_1^1 r_l^2 \, \mathbb{1}_{(0,\rho]}(r_l). \tag{11}$$

For $s = 2$, define first the function:

$$h_k(x, y) = \frac{\pi}{2} + (-1)^k \arccos\left(\frac{x}{2\rho \sin y}\right), \quad k = 1, 2 \tag{12}$$

which, according to $\mathbf{Z}_2$ in (3), allows one to express ϕ_l as a function of r_l and θ_l, and then θ_l as a function of r_l, with the aim of expressing the corresponding pdf of R_l as:

$$f_{R_l}(r_l; 2) = \frac{3r_l^2}{4\pi\rho^3} \int_{h_1(r_l,\pi/2)}^{h_2(r_l,\pi/2)} \left(\int_{h_1(r_l,\theta_l)}^{h_2(r_l,\theta_l)} \mathrm{d}\phi_l\right) \sin\theta_l \mathrm{d}\theta_l. \tag{13}$$

By solving this integral and manipulating, one obtains:

$$f_{R_l}(r_l; 2) = \left[\sum_{n=1}^{2} (n+2) a_n^2 r_l^{n+1}\right] \mathbb{1}_{(0,2\rho]}(r_l). \tag{14}$$

The integration of (11) and (14) on r_l, and the representation of the results in compact form finally provides (9). □

Purpose of the second step is to model the impact of path-loss attenuation and shadowing by deriving the cdf of the rv:

$$Q_l = \frac{P_T \Psi_l}{\alpha R_l^{\beta}}, \quad l = 1,\dots,L \tag{15}$$

To this aim, the following lemma is formulated.

Lemma 2 (Cdf and pdf of Q_l): Let Ψ_l be distributed according to (5) and R_l according to (9)-(10). Let $\varpi = \alpha/P_T$ and $\chi_s = 1/[\varpi(s\rho)^{\beta}]$. Then, for $s = 1, 2$ and $l = 1,\dots,L$, the cdf and pdf of Q_l in (15) are given, respectively, by:

$$F_{Q_l}(q_l; s) = \left[\sum_{n=0}^{2} \tilde{a}_n^s V_n^s(q_l)\right] \mathbb{1}_{\mathbb{R}_{>0}}(q_l), \tag{16a}$$

$$f_{Q_l}(q_l; s) = \left[\sum_{n=0}^{2} \tilde{a}_n^s \frac{W_n^s(q_l) - b_n V_n^s(q_l)}{q_l}\right] \mathbb{1}_{\mathbb{R}_{>0}}(q_l), \tag{16b}$$

where, for $n = 0, 1, 2$, the following definitions hold:

$$V_n^s(x) = \frac{1}{x^{b_n}}\left\{1 - \operatorname{erf}\left[\frac{b_n}{\sqrt{2}} + \frac{1}{\sqrt{2}\tilde{\sigma}} \log\left(\frac{\chi_s}{x}\right)\right]\right\}, \tag{17a}$$

$$W_n^s(x) = \frac{\sqrt{2}}{\sqrt{\pi}\tilde{\sigma}x^{b_n}} \exp\left\{-\frac{1}{2}\left[b_n + \frac{1}{\tilde{\sigma}}\log\left(\frac{\chi_s}{x}\right)\right]^2\right\}, \quad (17b)$$

$$\tilde{a}_n^s = \frac{1}{2}\left\{\delta_{n,0} - \frac{1-\delta_{n,0}}{\varpi^{\frac{n+2}{\beta}}} \exp\left[\frac{(10-n)\tilde{\sigma}^2}{(3-n)\beta^2}\right] a_n^s\right\}, \quad (17c)$$

$$b_n = \frac{n(4-n)\tilde{\sigma}}{\beta}. \quad (17d)$$

Proof: Define the rv $T_l = 1/(\varpi R_l^\beta)$, which, by (9), has cdf:

$$F_{T_l}(t_l; s) = \Pr\{T_l \le t_l\} = 1 - F_{R_l}\left[(\varpi t_l)^{-\frac{1}{\beta}}\right] = \left[1 - \sum_{n=1}^{2} a_n^s (\varpi t_l)^{-\frac{n+2}{\beta}}\right] \mathbb{1}_{[\chi_s, +\infty)}(t_l). \quad (18)$$

Using (5) and (18), the cdf of $Q_l = T_l \Psi_l$ may be then obtained from the product distribution by solving the integral [6]:

$$F_{Q_l}(q_l; s) = \int_0^{+\infty} F_{T_l}\left(\frac{q_l}{\psi_l}; s\right) f_{\Psi_l}(\psi_l) \mathrm{d}\psi_l, \quad (19)$$

which, after some manipulations, leads to (16)-(17). □

The third step provides the average capacity of the $\mathrm{S}_1 - \mathrm{D}$ link from the coverage probability and the cdf of the interference. This latter quantity is estimated by adopting the strongest interferer approximation [3], in order to realistically consider the different signals subject to individual channel realizations. Accordingly, we can formulate the following proposition.

Proposition 1 (Average link capacity): Let $\mathcal{L}$ be distributed according to (1), G_{N_l} according to (6)-(7) for $\mathrm{N} \in \{\mathrm{T}, \mathrm{R}\}$, and Q_l according to (16)-(17). Then, for $s, m = 1, 2$, the average link capacity may be estimated by:

$$C_m(\xi; s) \cong \frac{\mathcal{M}_m(\xi)}{\mathfrak{g}^2} \mathbb{E}_{\mathcal{L}} \left\{ \int_{\xi\mathcal{N}}^{+\infty} \left[\sum_{n=0}^{2} \frac{\mathfrak{g}^n c_1^n}{\mathfrak{G}^n} f_{Q_l}\left(\frac{p_1}{\mathfrak{G}^n \mathfrak{g}^{2-n}}; s\right)\right] \cdot \left[\sum_{n=0}^{2} c_{l\neq 1}^n F_{Q_l}\left(\frac{p_1 - \xi\mathcal{N}}{\mathfrak{G}^2 \mathfrak{g}^{2-n}\xi}; s\right)\right]^{L-1} \mathrm{d}p_1 \right\}, \quad (20)$$

where:

$$c_l^n = (1 + \delta_{n,1}) K_l^n(\Omega) \left[1 - K_l(\Omega)\right]^{2-n}, \quad n = 0, 1, 2. \quad (21)$$

Proof: Define first the rv $G_l = G_{\mathrm{T}_l} G_{\mathrm{R}_l}$, whose pdf can be calculated from the product distribution as:

$$F_{G_l}(g_l) = \int_{\mathfrak{g}}^{\mathfrak{G}} f_{G_{\mathrm{R}_l}}\left(\frac{g_l}{g_{\mathrm{T}_l}}\right) \frac{f_{G_{\mathrm{T}_l}}(g_{\mathrm{T}_l})}{g_{\mathrm{T}_l}} \mathrm{d}g_{\mathrm{T}_l} = \sum_{n=0}^{2} c_l^n \delta\left(g_l - \frac{\mathfrak{G}^n}{\mathfrak{g}^{n-2}}\right), \quad (22)$$

by using (6) and exploiting the scaling and translation properties of the Dirac delta function. From this latter pdf one can evaluate the cdf of $P_l = G_l Q_l$ in (4). Applying again the product distribution, one directly obtains:

$$F_{P_l}(p_l; s) = \int_{\mathfrak{g}^2}^{\mathfrak{G}^2} F_{Q_l}\left(\frac{p_l}{q_l}; s\right) f_{G_l}(g_l) \mathrm{d}g_l = \sum_{n=0}^{2} c_l^n \, F_{Q_l}\left(\frac{p_l}{\mathfrak{G}^n \mathfrak{g}^{2-n}}; s\right). \quad (23)$$

TABLE I
ADOPTED PARAMETERS [4], [7]

ρ	100 m	$\mathfrak{g}$	0 dB	β	2.0 (LOS)
P_{T}	0 dBW	$\mathcal{N}$	-74.0 dBm		2.9 (NLOS)
$\Omega = 3\hat{\sigma}$	$\pi/4$ sr	α	61.4 dB (LOS)	$\tilde{\sigma}$	5.8 dB (LOS)
$\mathfrak{G}$	20 dB		72.0 dB (NLOS)		8.7 dB (NLOS)

The rv U, describing the interference plus noise power, may be then estimated adopting the strongest interferer approximation [3], according to which $U \cong \max(P_2, \ldots, P_L) + \mathcal{N}$. Hence, recalling the rules for the maximum and the translation of rvs, the conditional cdf of U given $\mathcal{L}$ can be expressed as:

$$F_{U|\mathcal{L}}(u|L; s) \cong F_{P_{l\neq 1}}^{L-1}(u - \mathcal{N}; s). \quad (24)$$

For $l = 1$, the pdf of the desired signal power P_1 can be immediately obtained from (23) as:

$$f_{P_1}(p_1; s) = \frac{\mathrm{d}F_{P_1}}{\mathrm{d}p_1} = \sum_{n=0}^{2} \frac{c_1^n}{\mathfrak{G}^n \mathfrak{g}^{2-n}} f_{Q_l}\left(\frac{p_1}{\mathfrak{G}^n \mathfrak{g}^{2-n}}; s\right). \quad (25)$$

Since the coverage probability $\eta(\xi|L; s)$ is the complementary cdf of the SINR $\Xi = P_1/U$ given $\mathcal{L}$, one obtains:

$$\eta(\xi|L; s) = 1 - F_{\Xi|\mathcal{L}}(\xi|L; s) = \int_0^{+\infty} F_{U|\mathcal{L}}\left(\frac{p_1}{\xi}\middle| L; s\right) f_{P_1}(p_1; s) \mathrm{d}p_1, \quad (26)$$

by applying the ratio distribution. The average link capacity may be now estimated by removing the conditioning of (26) with respect to $\mathcal{L}$ and then multiplying the result by $\mathcal{M}_m(\xi)$ in (8) to account for the modulation. This yields:

$$C_m(\xi; s) = \mathcal{M}_m(\xi) \, \mathbb{E}_{\mathcal{L}}[\eta(\xi|L; s)], \quad (27)$$

which, by substituting (23)-(26), finally provides (20). □

As desired, the obtained estimation of the average link capacity includes the destination's location, being (20) dependent on the parameter s. Besides, interestingly, the calculation of $C_m(\xi; s)$ requires just one numerical integration, since the statistics of U and P_1 are derived in analytical form. The insights inferable from this analysis together with its validation are presented in the next section.

IV. RESULTS

The results are derived using the parameters in Table I, which refers to the 28 GHz channel in line-of-sight (LOS) and non-LOS (NLOS) conditions [4]. The noise power $\mathcal{N}$ is evaluated considering the thermal noise power spectral density of -174 dBm/Hz for a receiver having a bandwidth of 1 GHz and a noise figure of 10 dB. The theoretical curves are represented by lines and validated by independent Monte Carlo simulations, which are instead represented by markers.

The first set of results shows the coverage probability as a function of the required SINR at the center and at the boundary of $\mathbf{B}(O, \rho)$ in LOS/NLOS conditions for $L = 10$ and $L = 100$ (Fig. 2). As expected, for a given location and a given propagation environment, the increase of the number of active

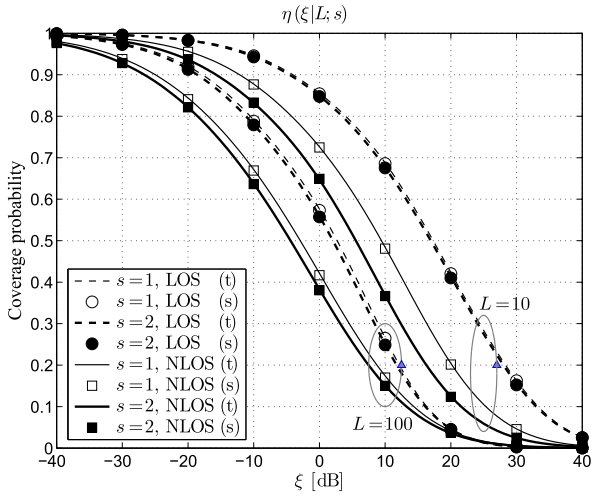

Fig. 2. Coverage probability as a function of the required SINR at the center ($s=1$) and at the boundary ($s=2$) of the cell in LOS and NLOS conditions for $L=10$ and $L=100$ active sources (t: theory, s: Monte Carlo simulation).

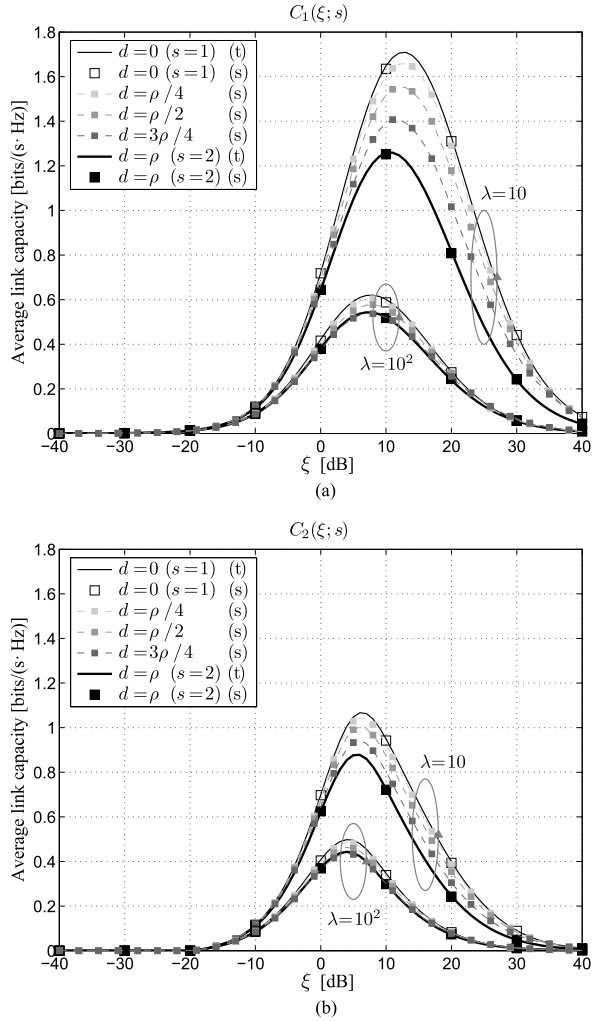

Fig. 3. Average link capacity as a function of the required SINR in NLOS conditions for $\lambda=10$ and $\lambda=10^2$ average active sources when D is placed at different distances d from O: (a) Shannon bound, (b) QPSK modulation (t: theory, s: Monte Carlo simulation).

pairs reduces the coverage probability because of the larger interference suffered by the target link. Besides, for fixed L and s values, the LOS scenario is preferable to the NLOS one, since, in the first case, S_1 is received by D with a higher power. Concerning the impact of the destination's location, it is interesting to observe that, for a given L value and a given propagation environment, $\eta(\xi|L;1)$ is always larger or equal to $\eta(\xi|L;2)$. This occurs because, according to (3), the statistical location of S_l with respect to D ranges from 0 to ρ for $s=1$ and from 0 to 2ρ for $s=2$. Thus, when D is located at the boundary of the cell, not only its interferers are statistically farther, but also, and more importantly, its target source.

The above considerations are deepened by Fig. 3, which reports the average link capacity as a function of the required SINR for different values of the distance d between D and O. The figure focuses on the NLOS case for $\lambda=10$ and $\lambda=100$ using the Shannon bound (Fig. 3(a)) and the QPSK modulation (Fig. 3(b)). When the m and λ values are given, the curves corresponding to $s=1$ and $s=2$ may be seen as the bounds of a region identifying the range of variation of $C_m(\xi;s)$ with respect to the position of D. The wider this region, the stronger the impact of the destination's location on the link performance, which in fact results significant for not too dense scenarios ($\lambda=10$). Conversely, the shrinking of this region for $\lambda=100$ shows that, in dense networks, the interference effects tend to prevail over those due to the location of D. The additional simulations carried out for the intermediate positions puts finally into evidence that the $C_m(\xi;s)$ gap from $d=0$ to $d=\rho/4$ is lower than that from $d=3\rho/4$ to $d=\rho$, thus revealing a faster capacity reduction as the destination becomes closer to the boundary of the cell.

V. Conclusion

A 3D analysis of the average link capacity achievable by an interfered P2P mmWave communication with a boundary located destination has been presented. The theoretical results, validated by independent Monte Carlo simulations, have revealed that the NLOS scenario is in general more sensitive to the destination's position, whose influence remains relevant until the network does not become too dense.

References

[1] J. G. Andrews *et al.*, "What will 5G be?" *IEEE J. Sel. Areas Commun.*, vol. 32, no. 6, pp. 1065–1082, Jun. 2014.

[2] V. Naghshin, A. M. Rabiei, N. C. Beaulieu, and B. Maham, "Accurate statistical analysis of a single interference in random networks with uniformly distributed nodes," *IEEE Commun. Lett.*, vol. 18, no. 2, pp. 197–200, Feb. 2014.

[3] F. Babich and M. Comisso, "Including the angular domain in the analysis of finite multi-packet peer-to-peer networks with uniformly distributed sources," *IEEE Trans. Commun.*, vol. 64, no. 6, pp. 2494–2510, Jun. 2016.

[4] M. R. Akdeniz *et al.*, "Millimeter wave channel modeling and cellular capacity evaluation," *IEEE J. Sel. Areas Commun.*, vol. 32, no. 6, pp. 1164–1179, Jun. 2014.

[5] V. M. Nguyen and M. Kountouris, "Performance limits of network densification," *IEEE J. Sel. Areas Commun.*, vol. 35, no. 6, pp. 1294–1308, Jun. 2017.

[6] R. D. Yates and D. J. Goodman, *Probability and Stochastic Processes*. Hoboken, NJ, USA: Wiley, 1999.

[7] M. D. Renzo, "Stochastic geometry modeling and analysis of multi-tier millimeter wave cellular networks," *IEEE Trans. Wireless Commun.*, vol. 14, no. 9, pp. 5038–5057, Sep. 2015.

[8] F. Babich, A. Soranzo, and F. Vatta, "Useful mathematical tools for capacity approaching codes design," *IEEE Commun. Lett.*, vol. 21, no. 9, pp. 1949–1952, Sep. 2017.